X-ray optics simulation using Gaussian superposition technique

Mourad Idir,[1,*] Moisés Cywiak,[2] Arquímedes Morales,[2] and Mohammed H. Modi[3]

[1]*Brookhaven National Laboratory – NSLS II 50 Rutherford Dr. Upton 11973-5000, New York, USA*
[2]*Centro de Investigaciones en Óptica A.C.Loma del Bosque No. 115 León Gto., Mexico*
[3]*X-ray Optics Section, Raja Ramanna, Centre for Advanced Technology, Indore 452013, India*
**midir@bnl.gov*

Abstract: We present an efficient method to perform x-ray optics simulation with high or partially coherent x-ray sources using Gaussian superposition technique. In a previous paper, we have demonstrated that full characterization of optical systems, diffractive and geometric, is possible by using the Fresnel Gaussian Shape Invariant (FGSI) previously reported in the literature. The complex amplitude distribution in the object plane is represented by a linear superposition of complex Gaussians wavelets and then propagated through the optical system by means of the referred Gaussian invariant. This allows ray tracing through the optical system and at the same time allows calculating with high precision the complex wave-amplitude distribution at any plane of observation. This technique can be applied in a wide spectral range where the Fresnel diffraction integral applies including visible, x-rays, acoustic waves, etc. We describe the technique and include some computer simulations as illustrative examples for x-ray optical component. We show also that this method can be used to study partial or total coherence illumination problem.

OCIS codes: (340.0340) X-ray optics; (340.7470) X-ray mirrors; (340.6720) Synchrotron radiation.

References and links

1. B. Lai and F. Cerrina, "SHADOW: A synchrotron radiation ray tracing program," Nucl. Instrum. Methods Phys. Res. A **246**(1-3), 337–341 (1986).
2. T. Moreno and M. Idir, "SPOTX a ray tracing software for X-ray optics," J. Phys. (France) **11**, 527–531 (2001).
3. T. Yamada, N. Kawahara, M. Doi, T. Shoji, N. Tsuruoka, and H. Iwasaki, "A new ray-tracing program RIGTRACE for X-ray optical systems," J. Synchrotron Radiat. **8**(3), 1047–1050 (2001).
4. F. Schafers, "The BESSY ray trace programm: Ray," *Modern Developments in X-Ray and Neutron Optics*, A. Erko, M. Idir, T. Krist, and A. G. Michette, eds. (Springer Science2008), p. 9.
5. M. Bowler, J. Bahrdt, and O. Chubar, "Wavefront propagation," *Modern Developments in X-Ray and Neutron Optics* (Springer Series in Optical Sciences, 2008), pp. 69–90.
6. K. Yamauchi, K. Yamamura, H. Mimura, Y. Sano, A. Saito, K. Endo, A. Souvorov, M. Yabashi, K. Tamasaku, T. Ishikawa, and Y. Mori, "Wave-optical evaluation of interference fringes and wavefront phase in a hard-x-ray beam totally reflected by mirror optics," Appl. Opt. **44**(32), 6927–6932 (2005).
7. C. M. Kewish, L. Assoufid, A. T. Macrander, and J. Qian, "Wave-optical simulation of hard-x-ray nanofocusing by precisely figured elliptical mirrors," Appl. Opt. **46**(11), 2010–2021 (2007).
8. M. H. Modi, M. Idir, R. Garrett, I. Gentle, K. Nugent, S. Wilkins, and M. Idir, "Shape error analysis for reflective nano focusing optics,", SRI 2009," AIP Conf. Proc. 1234, 681–684 (2010).
9. M. Cywiak, M. Servín, and F. Mendoza-Santoyo, "Wave-front propagation by Gaussian superposition," Opt. Comm. **195**(5–6), 351–359, (2001).
10. M. Cywiak, A. Morales, M. Servín, and R. Gómez-Medina, "A technique for calculating the amplitude distribution of propagated fields by Gaussian sampling," Opt. Express **18**(18), 19141–19155 (2010), http://www.opticsinfobase.org/oe/abstract.cfm?URI=oe-18-18-19141.
11. M. Cywiak, A. Morales, J. M. Flores, and M. Servín, "Fresnel-Gaussian shape invariant for optical ray tracing," Opt. Express **17**(13), 10564–10572 (2009), http://www.opticsinfobase.org/abstract.cfm?uri=oe-17-13-10564.
12. M. Cywiak, M. Servín, and A. Morales, "Diffractive and geometric optical systems characterization with the Fresnel Gaussian shape invariant," Opt. Express **19**(3), 1892–1904 (2011), http://www.opticsinfobase.org/oe/abstract.cfm?uri=oe-19-3-1892.

#149818 - $15.00 USD Received 23 Jun 2011; revised 3 Aug 2011; accepted 3 Aug 2011; published 15 Sep 2011

13. I. A. Vartanyants, A. P. Mancuso, A. Singer, O. M. Yefanov, and J. Gulden, "Coherence measurements and coherent diffractive imaging at FLASH," J. Phys. At. Mol. Opt. Phys. **43**(19), 194016 (2010).
14. F. Livet, "Diffraction with a coherent X-ray beam: dynamics and imaging," Acta Crystallogr. A **63**(2), 87–107 (2007).
15. W. Leitenberger, S. M. Kuznetsov, and A. Snigirev, "Interferometric measurements with hard X-rays using a double slit," Opt. Commun. **191**(1–2), 91–96 (2001).
16. T. Ditmire, E. T. Gumbrell, R. A. Smith, J. W. Tisch, D. D. Meyerhofer, and M. H. Hutchinson, "Spatial coherence measurement of soft X-ray radiation produced by high order harmonic generation," Phys. Rev. Lett. **77**(23), 4756–4759 (1996).
17. Y. Liu, Y. Wang, M. A. Larotonda, B. M. Luther, J. J. Rocca, and D. T. Attwood, "Spatial coherence measurements of a 13.2 nm transient nickel-like cadmium soft x-ray laser pumped at grazing incidence," Opt. Express **14**(26), 12872–12879 (2006), http://www.opticsinfobase.org/abstract.cfm?id=121404.
18. M. Howells, C. Jacobsen, and T. Warwick, "Principles and applications of zone plate X-ray microscopes," in *Science of Miscrocopy*, Eds. Peter W. Hawkes & John C.H. Spence, XXXVI, (Springer, 2007).
19. W. Chao, B. D. Harteneck, J. A. Liddle, E. H. Anderson, and D. T. Attwood, "Soft X-ray microscopy at a spatial resolution better than 15 nm," Nature **435**(7046), 1210–1213 (2005).
20. W. Chao, J. Kim, S. Rekawa, P. Fischer, and E. H. Anderson, "Demonstration of 12 nm resolution Fresnel zone plate lens based soft x-ray microscopy," Opt. Express **17**(20), 17669–17677 (2009), http://www.opticsinfobase.org/abstract.cfm?uri=oe-17-20-17669.
21. G. Schneider, P. Guttmann, S. Heim, S. Rehbein, F. Mueller, K. Nagashima, J. B. Heymann, W. G. Müller, and J. G. McNally, "Three-dimensional cellular ultrastructure resolved by X-ray microscopy," Nat. Methods **7**(12), 985–987 (2010).
22. K. Iizuka, *Engineering Optics*, (Springer Series in Optical Sciences, 1986), Ch. 4.
23. A. Snigirev, V. Kohn, I. Snigireva, and B. Lengeler, "A compound refractive lens for focusing high-energy X-rays," Nature **384**(6604), 49–51 (1996).
24. T. Tomie, "The birth of the X-ray refractive lens," Spectrochim. Acta, B At. Spectrosc. **65**(3), 192–198 (2010).
25. A. Snigirev, V. Kohn, I. Snigireva, A. Souvorov, and B. Lengeler, "Focusing high-energy x rays by compound refractive lenses," Appl. Opt. **37**(4), 653–662 (1998).
26. C. G. Schroer, P. Boye, J. M. Feldkamp, J. Patommel, A. Schropp, A. Schwab, S. Stephan, M. Burghammer, S. Schöder, and C. Riekel, "Coherent x-ray diffraction imaging with nanofocused illumination," Phys. Rev. Lett. **101**(9), 090801 (2008).

1. Introduction

In recent years a steadily growing interest has been made in the design of electron accelerators in order to reduce the beam emittance and to increase the photon brilliance. This has increased the coherent properties of the beam and has opened up new branches of microscopy and spectroscopy at nano meter length scales. X-ray nano probe is going to be an important tool for future research, hence numerous work have been carried out to develop nano focusing optics of diffraction limited performance. However, there is no simple way to describe the wave-front propagation through x-ray optical component. Traditionally, Monte Carlo ray tracing, based on geometric optics, has been used to model the x-ray components that transport the x-ray beam radiation from the source to the sample [1,2]. With these new installations, these simulations tools cannot be used to accurately simulate the high or partially coherent beam and wave-optical calculations are essential for predicting the x-ray optics performances [3–8].

In this paper, we will use wavefront propagation by Gaussian superposition to simulate some x-ray optical components. The presented technique can be used to characterize from simple (slit, double slits) to more complex x-ray optical components (Fresnel zone plate (FZP), refractive lenses and mirrors) using full or partial coherence of the incoming beam. Our proposed technique is based in the propagation of a Gaussian shape invariant under the Fresnel diffraction integral [9–12]. This paper is organized as follows. In Section 2, we outline the mathematical description of the Gaussian superposition technique and in Section 3 we describe its applicability to problems related to x-ray optics simulation and show some simulation results and discussion. Finally, conclusions are drawn in Section 4.

#149818 - $15.00 USD Received 23 Jun 2011; revised 3 Aug 2011; accepted 3 Aug 2011; published 15 Sep 2011

2. Theoretical framework - Mathematical description of the Gaussian superposition technique

In this section we give a short overview of the simulation tools used. Our method is divided in two approaches:

2.1 Gaussian superposition

The Gaussian superposition can be applied for the Young slits and for the FZP propagation. This is because rays are not needed here. Thus, the front-wave is sampled and Fresnel propagated.

Let an object field being located at a coordinate plane (x, y). We will represent this wavefront as a superposition of Gaussian wavelets equally spaced following a Rayleigh-like criterion, with each wavelet having the same semi-width describe by

$$\Psi_0(x,y) = \sum_m P_m \exp\left(-\frac{(x-x_m)^2+(y-y_m)^2}{\sigma^2}\right)\exp\left(i\alpha_m(x^2+y^2)\right)\exp\left(i\beta_m(x+y)\right). \quad (1)$$

In Eq. (1), σ is the semi-width of each Gaussian wavelet in the superposition process. α_m, β_m represent defocus and tilting factors respectively. The spatial centers of each Gaussian function are located at (x_m, y_m) and P_m are the amplitudes of each Gaussian wavelet, selected as the height of its corresponding pixel.

To calculate the amplitude distribution of the propagated wave-front at a coordinate plane (ξ,η), parallel to the (x, y) plane, located at a distance z from the object plane, we will use the Fresnel diffraction integral given by,

$$\Psi_P(\xi,\eta) = \frac{1}{i\lambda z}\int_{-\infty}^{\infty}\int_{-\infty}^{\infty}\Psi_0(x,y)\exp\left(i\frac{\pi}{\lambda z}\left[(x-\xi)^2+(y-\eta)^2\right]\right)dx\,dy. \quad (2)$$

Substituting Eq. (1) into Eq. (2) gives the amplitude distribution of the propagated field

$$\begin{aligned}\Psi_{PROP}(\xi,\eta) = -i\sum_{m=0}^{M} P_m(\lambda z + ia)\frac{\pi\sigma^2}{d}\exp\left(-\frac{x_m^2+y_m^2}{\sigma^2}+\frac{\lambda z p_m + a q_m}{\sigma^2\lambda z}+\frac{d(g_{xm}^2+g_{ym}^2)}{(\sigma\lambda z)^2}\right)\\ \times\exp\left(i\frac{\pi}{\lambda z}\left[\frac{d-\pi\sigma^2 a}{d}(\xi^2+\eta^2)-2(f_{xm}\xi+f_{ym}\eta)+\frac{\lambda z q_m - a p_m}{\pi\sigma^2}\right]\right) \quad (3)\\ \times\exp\left(-\frac{\pi^2\sigma^2}{d}\left[(\xi-\frac{dg_{xm}}{\pi\sigma^2\lambda z})^2+(\eta-\frac{dg_{ym}}{\pi\sigma^2\lambda z})^2\right]\right).\end{aligned}$$

In Eq. (3), for brevity we have defined,

$$\begin{aligned}&a_m = \sigma^2(\alpha_m\lambda z+\pi),\\ &d_m = \lambda^2 z^2 + a_m^2,\\ &f_{xm} = \frac{\lambda z}{2d_m}(2x_m\lambda z - \beta_m\sigma^2 a_m), \quad g_{xm} = \frac{\lambda z}{2d_m}(\beta_m\sigma^2\lambda z + 2x_m a_m), \quad (4)\\ &f_{ym} = \frac{\lambda z}{2d_m}(2y_m\lambda z - \beta_m\sigma^2 a_m), \quad g_{ym} = \frac{\lambda z}{2d_m}(\beta_m\sigma^2\lambda z + 2y_m a_m),\end{aligned}$$

and

#149818 - $15.00 USD Received 23 Jun 2011; revised 3 Aug 2011; accepted 3 Aug 2011; published 15 Sep 2011

$$p_m = f_x^2 m + f_{ym}^2 - g_{xm}^2 - g_{ym}^2,$$
$$q_m = 2(f_{xm} g_{xm} + f_{ym} g_{ym}). \tag{5}$$

Equations (3-5) will be used to calculate the amplitude distributions at a plane of observation for FZPs and Young slits diffraction where ray tracing is not necessary.

2.2 The Fresnel Gaussian Shape Invariant (which requires Gaussian superposition)

FGSI is necessary when tracing rays. For example, if we need to calculate the focusing performances of a reflective mirror, we need first to perform ray tracing. Then based in these rays, the diffraction pattern is calculated by means of FGSI.

For the cases where ray tracing is required, for example in refraction or reflection, we will apply the Gaussian superposition process to our FGSI in the following manner.

First, we represent each Gaussian wavelet at an arbitrary plane n as,

$$\Psi_n(x) = P_n \exp\left(i\alpha_n x\right)\exp\left(i\beta_n x^2\right)\exp\left(-\frac{\left(x - A_n\right)^2}{r_n^2}\right)\exp\left(i\gamma_n\left[x - B_n\right]^2\right). \tag{6}$$

By applying the Fresnel diffraction integral, Eq. (2) to Eq. (6), the amplitude distribution at a plane $n+1$ located at a distance z is given as,

$$\Psi_{n+1}(\xi, z) = P_{n+1}\exp\left(i\alpha_{n+1}\xi\right)\exp\left(i\beta_{n+1}\xi^2\right)$$
$$\exp\left(-\frac{\left(\xi - A_{n+1}\right)^2}{r_{n+1}^2}\right)\exp\left(i\gamma_{n+1}\left[\xi - B_{n+1}\right]^2\right). \tag{7}$$

In Eq. (7),

$$P_{n+1} = P_n \frac{\exp\left(i2\pi z/\lambda\right)}{\sqrt{i\lambda z}}\sqrt{\frac{\pi r_n^2 \lambda z}{\lambda z - i r_n^2\left(\beta_n \lambda z + \gamma_n \lambda z + \pi\right)}} \times$$
$$\exp\left(i\gamma_n B_n)^2\right)\exp\left(i\frac{\lambda z (A_n)^2}{r_n^4\left(\beta_n \lambda z + \gamma_n \lambda z + \pi\right)}\right),$$
$$\alpha_{n+1} = 0,\ \beta_{n+1} = \frac{\pi}{\lambda z},\ \gamma_{n+1} = -\frac{\pi^2 r_n^4}{D_n \lambda z}\left(\beta_n \lambda z + \gamma_n \lambda z + \pi\right),$$
$$r_{n+1} = \frac{\sqrt{D_n}}{\pi r_n}, \tag{8}$$
$$A_{n+1} = A_n + \frac{\alpha_n \lambda z}{2\pi} - \frac{\gamma_n \lambda z B_n}{\pi} + \frac{\left(\beta_n + \gamma_n\right)\lambda z A_n}{\pi},$$
$$B_{n+1} = \frac{\alpha_n \lambda z}{2\pi} - \frac{\gamma_n \lambda z B_n}{\pi} - \frac{\lambda^2 z^2}{\beta_n \lambda z + \gamma_n \lambda z + \pi}\frac{A_n}{\pi r_n^4},$$
$$D_n = \lambda^2 z^2 + r_n^4\left(\beta_n \lambda z + \gamma_n \lambda z + \pi\right)^2.$$

#149818 - $15.00 USD Received 23 Jun 2011; revised 3 Aug 2011; accepted 3 Aug 2011; published 15 Sep 2011

Each FGSI, aside of being part of the process of superposition, represents a traveling wavelet that can be viewed as a ray whose trajectory coincides with the spatial center of each FGSI. When a ray changes direction due to a reflection or refraction, to an angle θ_n it is necessary first to update the driver parameter α_n as,

$$\alpha_n = \frac{2\pi}{\lambda_n}\tan\left(\theta_n\right), \tag{9}$$

and then, accordingly,

$$\begin{aligned} \alpha_{n+1} &= \frac{2\pi}{\lambda_{n+1}}\tan\left(\theta_n\right) + 2\gamma_{n+1}B_{n+1} - 2\left(\beta_{n+1} + \gamma_{n+1}\right)A_{n+1}, \\ P_{n+1} &= P_{n+1}\exp\left(-i\alpha_{n+1}A_{n+1}\right). \end{aligned} \tag{10}$$

After the overall ray tracing is performed, the superposition process is applied to calculate the diffraction pattern at the image plane.

The method suggested is based on the Fresnel integral transformations, this approximation results from paraxial conditions of the Fresnel integral, or, in other words, from parabolic differential equation (PDE) restrictions.

The principle of our technique for x-ray components simulation is illustrated by means of several different examples. In order to validate at least some of the modeling abilities of the program, it was decided to carry out a case study on typical x-ray components like, slits, double slits, diffractive lenses and refractive optics.

3. Application of the Gaussian superposition method to x-ray optics simulation

In this section we introduce several examples where different geometries and configurations of x-ray optical components are illustrated. These examples include single slit diffraction, Young slits interference experiment, x-ray diffractive lenses (Fresnel Zone Plate FZP).

3.1 Slit diffraction

The first example is the single slit diffraction with the aperture centered at x = 0 with a size equals to b = 20 microns. The incident wavefront is a plane wave and the wavelength used for this simulation is λ = 0.1 nm. Figure 1 shows the diffraction profile of a 20 micron slit versus the distance z between the slit and the detector.

#149818 - $15.00 USD Received 23 Jun 2011; revised 3 Aug 2011; accepted 3 Aug 2011; published 15 Sep 2011

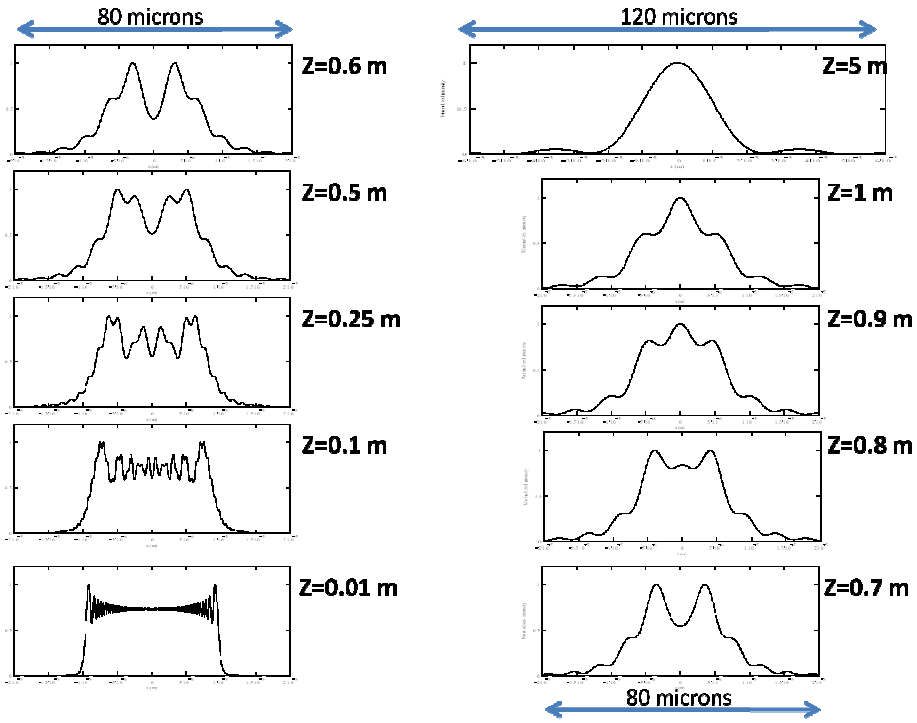

Fig. 1. 20 microns slit diffraction profile versus the distance z between the slit and the detector position for λ = 0.1 nm.

In Fig. 1, we clearly see the transition from Fresnel to Fraunhofer diffraction.

3.2 Young double slit modeling

In this example, the Young double slit experiment is modeled. The geometry is described in Fig. 2. The incident wavefront is a plane wave, and the wavelength used for this simulation is λ = 0.1 nm. The slit aperture is 5 microns and the center to center distance b = 30 microns.

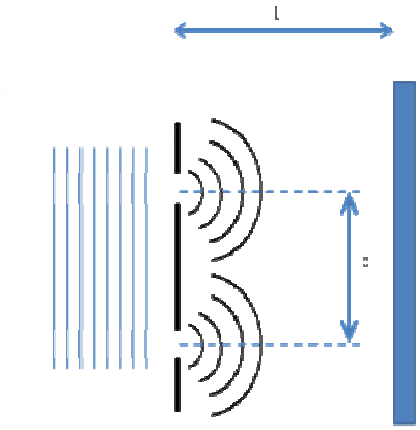

Fig. 2. Double slit diffraction geometry (slit size 5 microns, b = 30 microns and L vary from 1 cm to 300 cm)

Figure 3 shows the calculated interference patterns for several screens to slit distances.

#149818 - $15.00 USD Received 23 Jun 2011; revised 3 Aug 2011; accepted 3 Aug 2011; published 15 Sep 2011

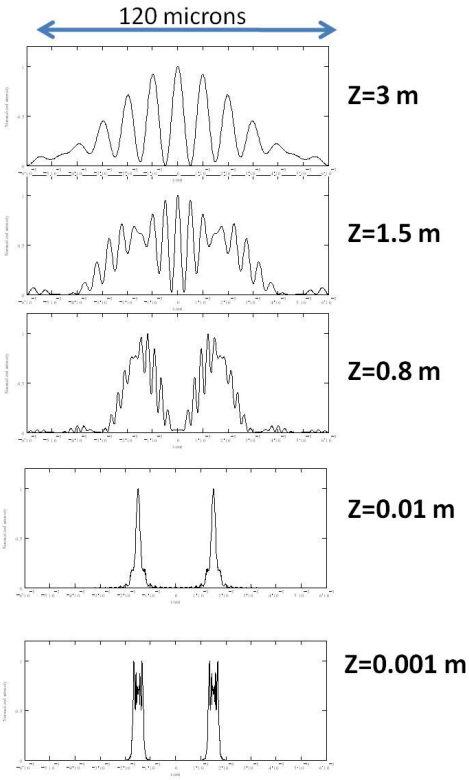

Fig. 3. Double Slit diffraction profile versus the distance z (from 1 mm up to 3 m) between the slit and the detector position for $\lambda = 0.1$ nm.

Our very powerful technique based on Wave-front propagation by Gaussian superposition can be used to simulate x-ray optical components under fully or partially coherent illumination. Young's double slit experiment is one of the most efficient and widely used methods for measuring the transverse coherence properties of wavefields [13]. Using the geometry describe in Fig. 4, we have calculated the normalized intensity distribution due to Young slits illuminated by two point sources with same intensity and variable coherence (from full to incoherent situation).

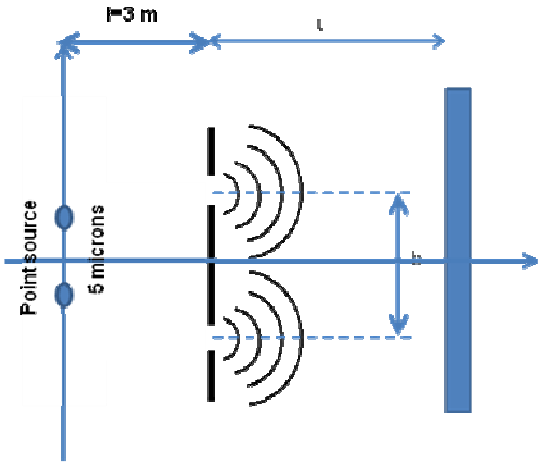

Fig. 4. Double Slit diffraction geometry using two points sources.

#149818 - $15.00 USD Received 23 Jun 2011; revised 3 Aug 2011; accepted 3 Aug 2011; published 15 Sep 2011

Two points source are separated by 5 microns and are illuminating two slits located at l = 3 m. The slit separation b is equal to 30 microns and the distance L where the detector is located varied from 30 cm to 3 m. The Coherence factor (COH) between the two sources is changed from fully coherent COH = 1 to fully incoherent COH = 0.

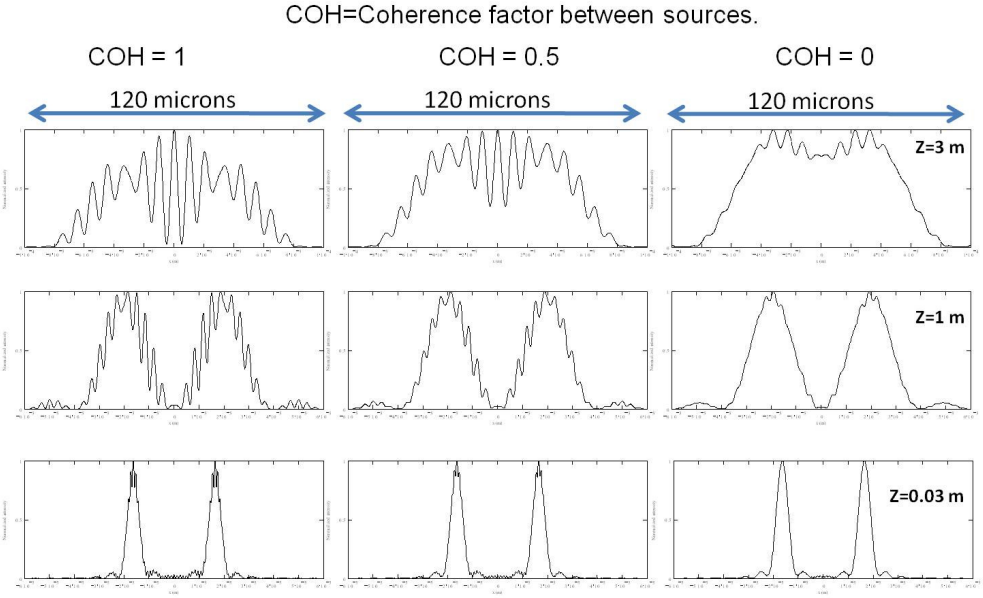

Fig. 5. Double Slit diffraction profile versus the distance z (from 1 mm up to 3 m) between the slit and the detector position for λ = 0.1 nm.

From Fig. 5, we can see that our model can be used to simulate interference patterns using x-ray partially coherent incoming beam. Some experimental results on x-ray pinhole diffraction [14] and hard and soft x-ray double slits experiments can be found in [15–17].

3.3 Focusing optics FZP – Refractive lenses

3.3.1 Fresnel zone plate

Among many x-ray microfocusing optics developed so far, FZPs have been demonstrated as one of the most promising for hard and soft x-ray spectral regions. FZPs are vastly used for X-rays focusing and are the key optical components in most x-ray microscopes [18–21]. The ultimate transverse spatial resolution δt for the m -th order diffraction on the focal plane is equal to $1.22\delta_N / m$, where the suffix N is the total number of zones and δ_N is the outermost zone width. In our simulation, we will assume that the FZP is illuminated by a plane wave so the focal point size will be diffraction limited and equal to $1.22\delta_N / m$. We have chosen arbitrarily a zone plate with a principal focal length p = 1 m and a diameter D = 140 μm and an illuminating wavelength λ = 0.1nm (12.4 keV).

Our FZP is represented by the following equation,

$$ZP(x) = \frac{A}{2} + \sum_{n\neq 0} \frac{\sin(n\pi A/2)}{n\pi} \exp\left(-i \frac{2\pi n}{\lambda} \left[\sqrt{p^2 + x^2} - p \right] \right). \qquad (11)$$

In the Eq. (11), A is introduced to allow us to change the FZP duty cycle. When $A = 1$ the usual FZP is obtained, see for example [22]; we assign to this FZP a duty cycle of one or 100% in order to make easier the comparisons among different FZP. When $A < 1$, the duty cycle is less than one, for example, if $A = 0.9$, the FZP will exhibit a duty cycle of 0.9 or 90%

#149818 - $15.00 USD Received 23 Jun 2011; revised 3 Aug 2011; accepted 3 Aug 2011; published 15 Sep 2011

of the common FZP. For our simulations, the above equation is expressed as a superposition of Gaussian functions, and then propagated by means of the Fresnel diffraction integral.

Figure 6 shows the intensity distributions obtained at the first and second focal planes respectively for a FZP with a duty cycle of one. The width at the first focal plane is 0.2 μm FWHM with an integrated power of 0.12.

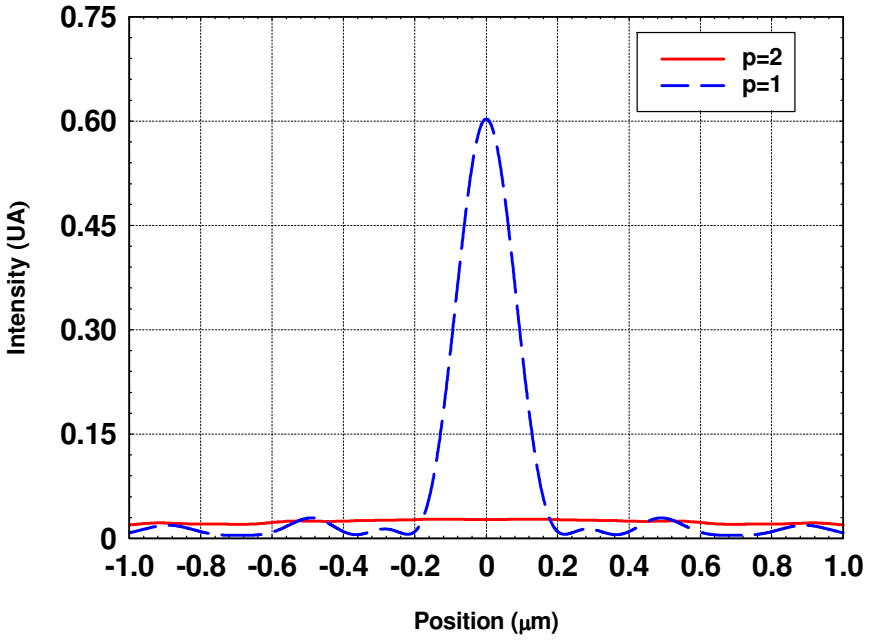

Fig. 6. Intensity distribution at the 1st and second focal plane (p = 1 and p = 2) for a ZP with duty cycle of one.

As anticipated because the duty cycle of the FZP is equal to 1, the second order diffraction is equal to zero. One possibility to overcome this problem is to modify the duty cycle. For example, Fig. 7 shows the intensity distributions at the first focal plane p = 1, and p = 1/2 respectively for a FZP with a duty cycle of 1/2 or 50%.

#149818 - $15.00 USD Received 23 Jun 2011; revised 3 Aug 2011; accepted 3 Aug 2011; published 15 Sep 2011

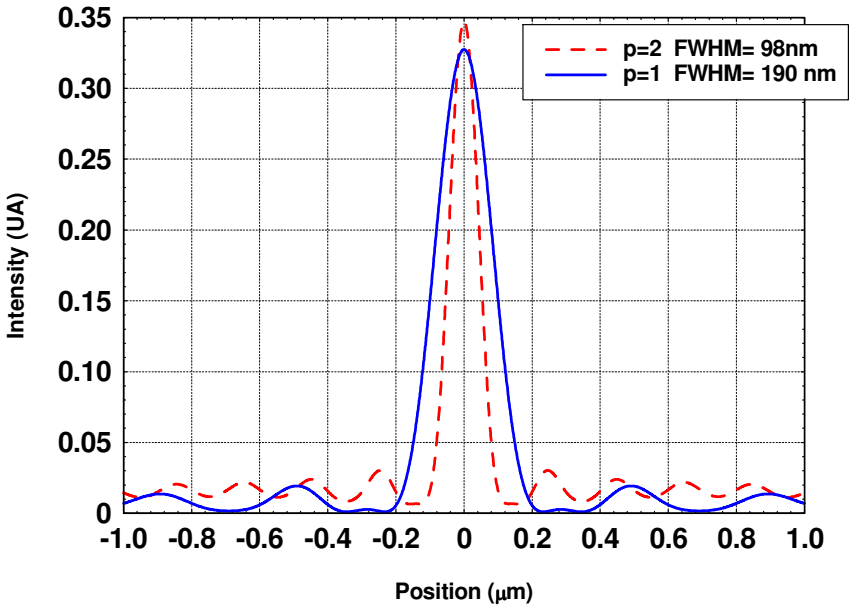

Fig. 7. Intensity distributions at the first and second focal plane (p = 1 and p = 2) for ZP with a duty cycle of 1/2.

For the 1st order diffraction, the total power under the central peak is 0.066 compare to the 0.12 (classical FZP). As it can be seen from the resulting figures, decreasing the duty cycle of the FZP improves the focusing performance without disturbing the principal focal region. Additionally, decreasing the duty cycle makes possible the use of the second order focal plane that normally cannot be used. With this approach, we can clearly see that the reduction of the duty cycle in a FZP results in a better focusing performance for the second order foci by reducing the FWHM of the focused spot size while maintaining reasonable efficiency.

3.3.2 Refractive lenses

Since the first successful observation [23,24] of synchrotron x-ray beam focusing with compound refractive lenses (CRL), the x-ray refractive optics was developed rapidly. Parabolic refractive x-ray lenses, made of light elements like beryllium and aluminum, are now commonly used as optical components for hard x-ray microscopy and analysis [25,26]. The parabolic profile guarantees that they image free of spherical aberrations.

In thin lens approximation, the focal distance of the lenses is given by $f = R/(2\delta N)$, where N is the number of single lenses and δ the index of refraction decrement ($n = 1-\delta + i\beta$). For Beryllium at $\lambda = 0.1$ nm, the index of refraction is (1-2.213e-6) + i3.177e-10. If we set R = 100 microns, the focal length can be expressed as: f (m) = 45.1875/N.

For our simulations, the geometry is described in Fig. 8.

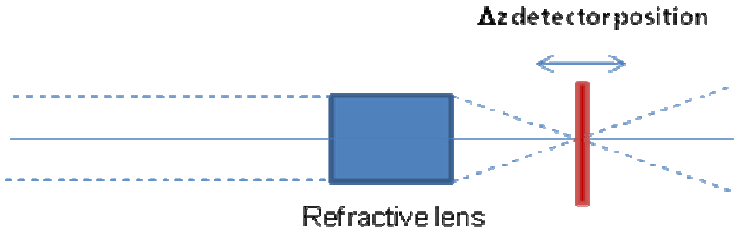

Fig. 8. Parabolic-Spherical Refractive lenses geometry. N = 1, f = 45.1875 m

#149818 - $15.00 USD Received 23 Jun 2011; revised 3 Aug 2011; accepted 3 Aug 2011; published 15 Sep 2011

Figure 9 shows the calculated diffraction pattern for N = 1 (f = 45.1875 m), R = 100 microns Be refractive lens. The lens exhibits double parabolic surfaces and the distance between surfaces is 10 microns.

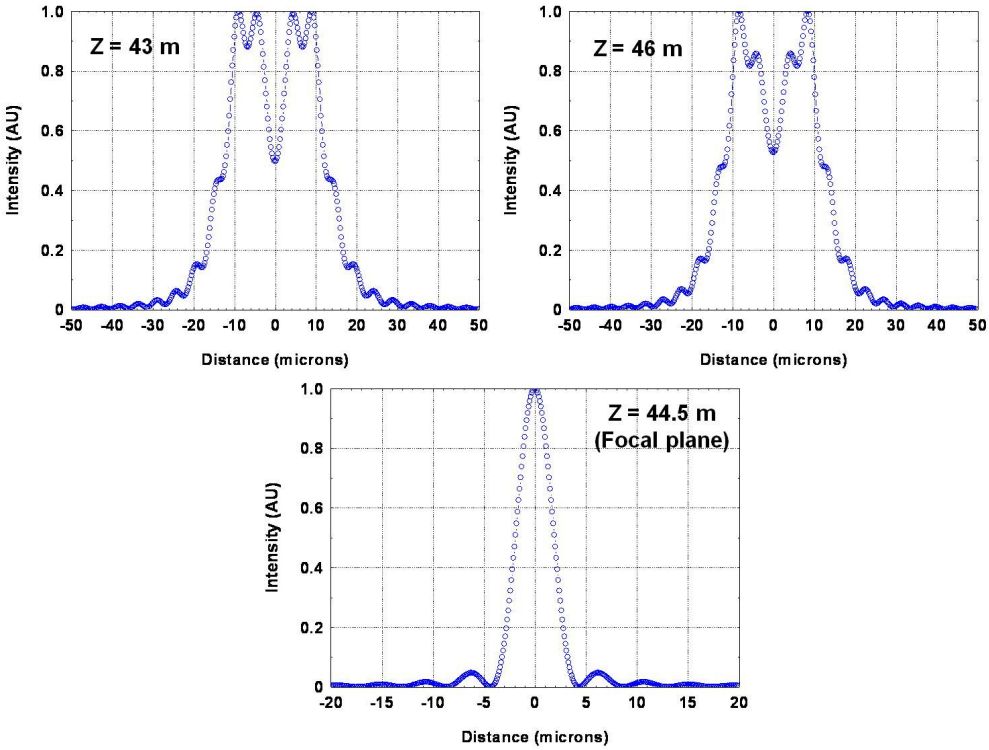

Fig. 9. Calculated diffraction pattern for a Be parabolic refractive lens (N = 1 (f = 2.2594 m), R = 100 microns).

4. Conclusions

We have demonstrated successful applications of our Gaussian superposition methods to simulate x-ray optical components from slits diffraction to x-ray lenses. These very powerful techniques based on wavefront propagation by Gaussian superposition can be used to simulate x-ray optics under fully or partially coherent illuminations. Our next step will be to use this technique in order to perform simulations of reflective optics and try more complex x-ray optical layout and compare our simulations with real measurements. We expect further applications of these interesting simulation tools.

Acknowledgments

This work was supported by the US Department of Energy, Office of Science, Office of Basic Energy sciences, under contract No. DE-AC-02-98CH10886.

#149818 - $15.00 USD Received 23 Jun 2011; revised 3 Aug 2011; accepted 3 Aug 2011; published 15 Sep 2011